Supplementary Information

Grain Boundary-Mediated Electrocatalytic C−N Coupling for Urea Synthesis from CO_2 and NO_x

Siqing Wang [a], Yan Zhang [a], Pengda Xiang [a], Dawei Chen [a, b, *], Qiling Li [c], Zhiyan Guo [a, *], Chen Chen [b, *]

a. College of Material Science and Engineering, Qingdao University of Science and Technology, Qingdao, China.

b. State Key Laboratory of Chem/Bio-Sensing and Chemometrics, College of Chemistry and Chemical Engineering, Hunan University, Changsha, China

c. College of Chemistry and Environmental Science, Qujing Normal University, Qujing, China

Correspondence and requests for materials should be addressed to Chen Chen (chenc@hnu.edu.cn), Dawei Chen (daweichen@qust.edu.cn), Zhiyan Guo (zhiyanguo@qust.edu.cn)

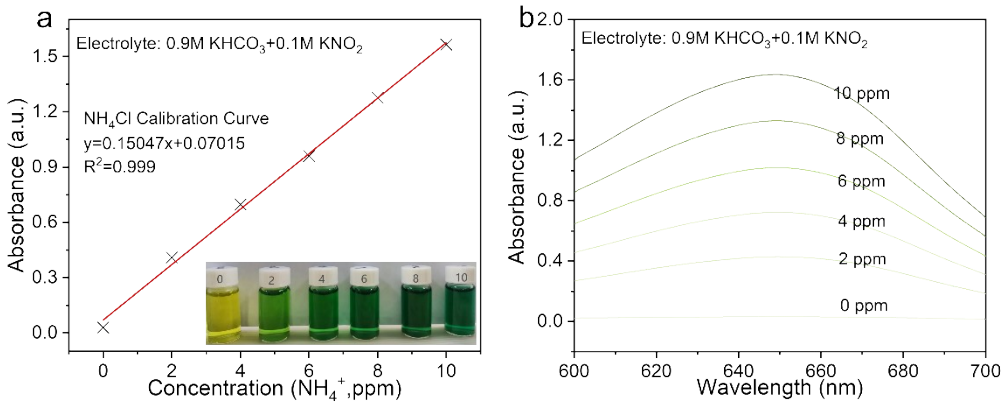

Figure S1. Calibration curves of NH_4^+ in 0.9 M $KHCO_3$ and 0.1 M KNO_2, and corresponding UV-vis absorption curves.

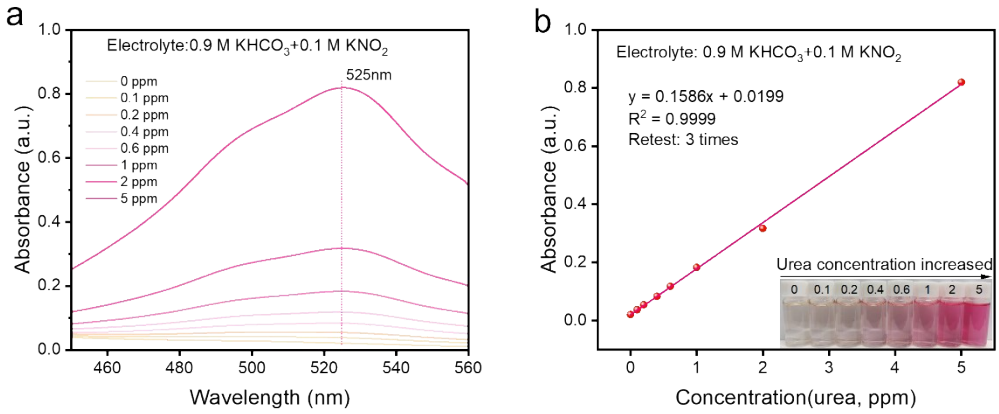

Figure S2. Calibration curves of urea determined by the diacetyl monoxime method in 0.9 M $KHCO_3$ and 0.1 M KNO_2 electrolyte, and corresponding UV-vis absorption spectra.

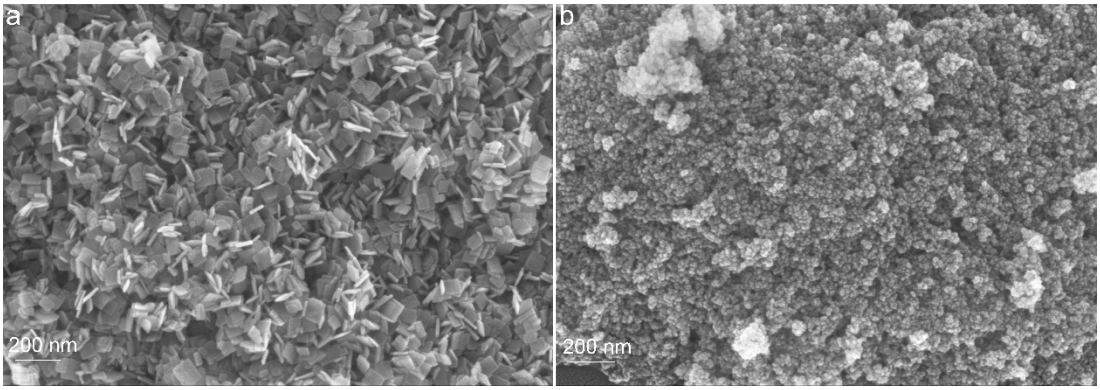

Figure S3. SEM images of a) TiO_2 b) GB-TiO_2

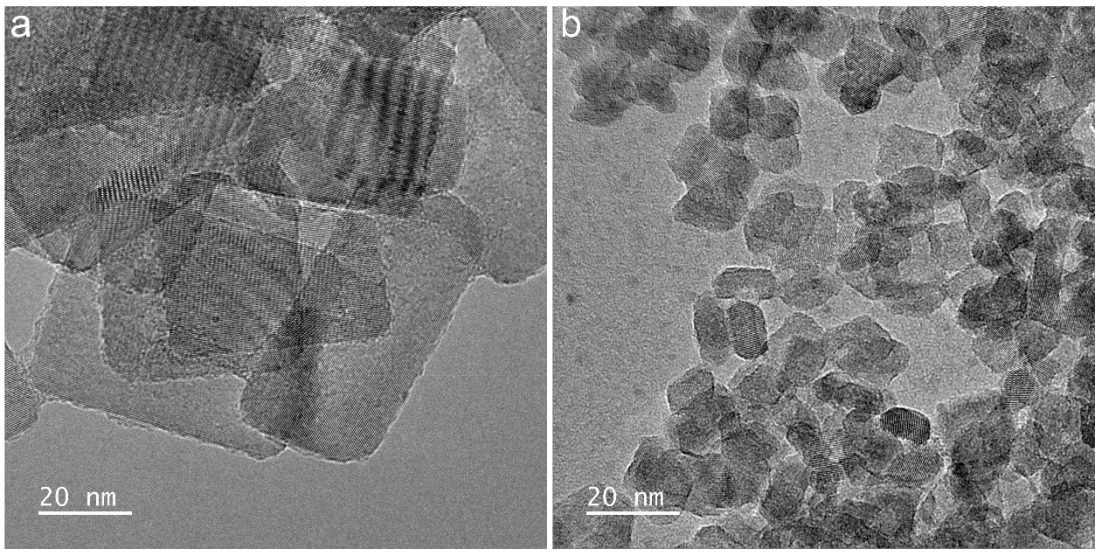

Figure S4. TEM images of a) TiO_2 b) GB-TiO_2

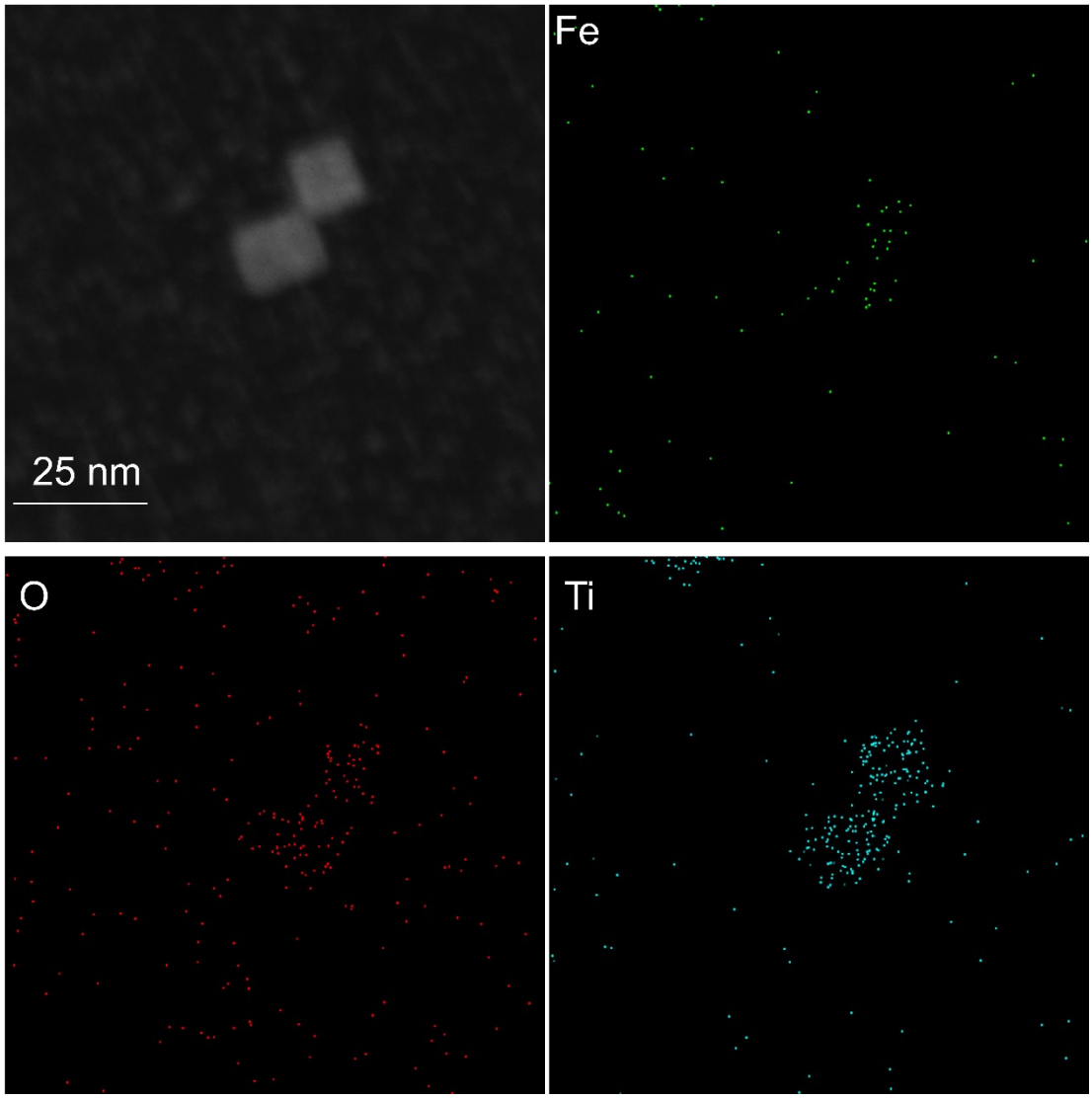

Figure S5. Elemental mapping images of GB-TiO_2

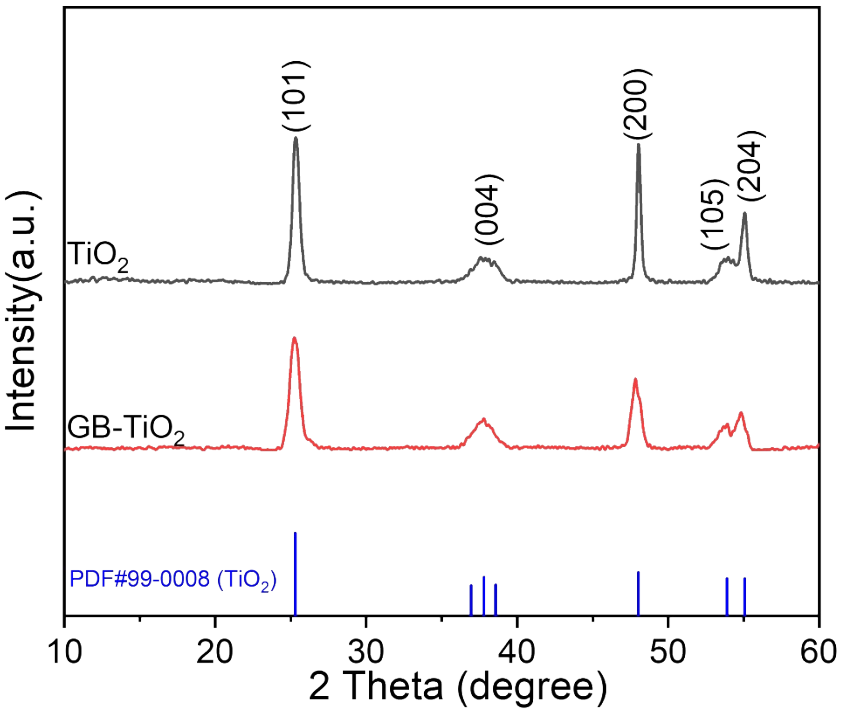

Figure S6. The XRD pattern of TiO_2 and GB-TiO_2.

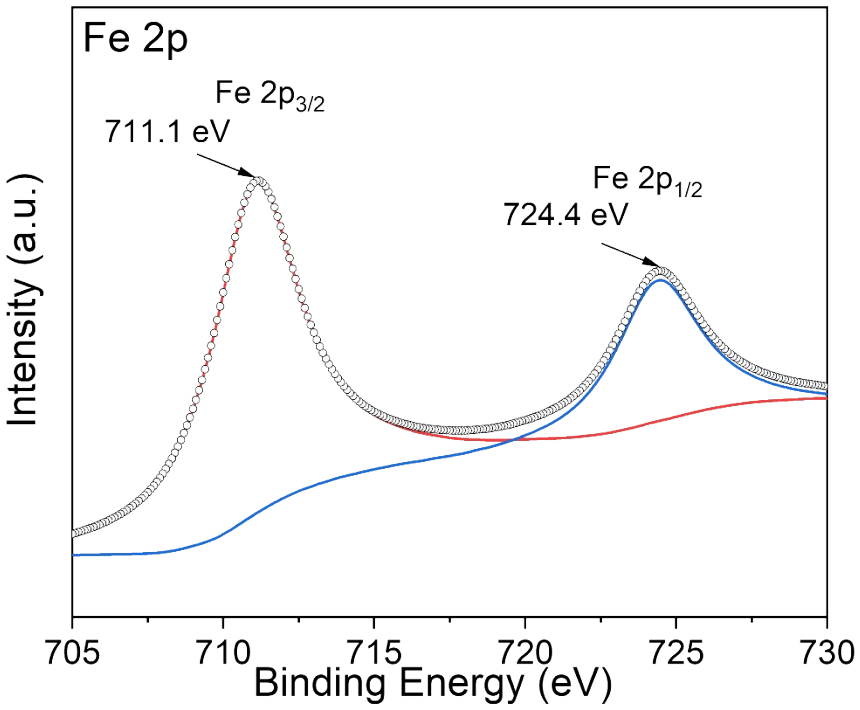

Figure S7. Fe 2p XPS spectra of GB-TiO_2.

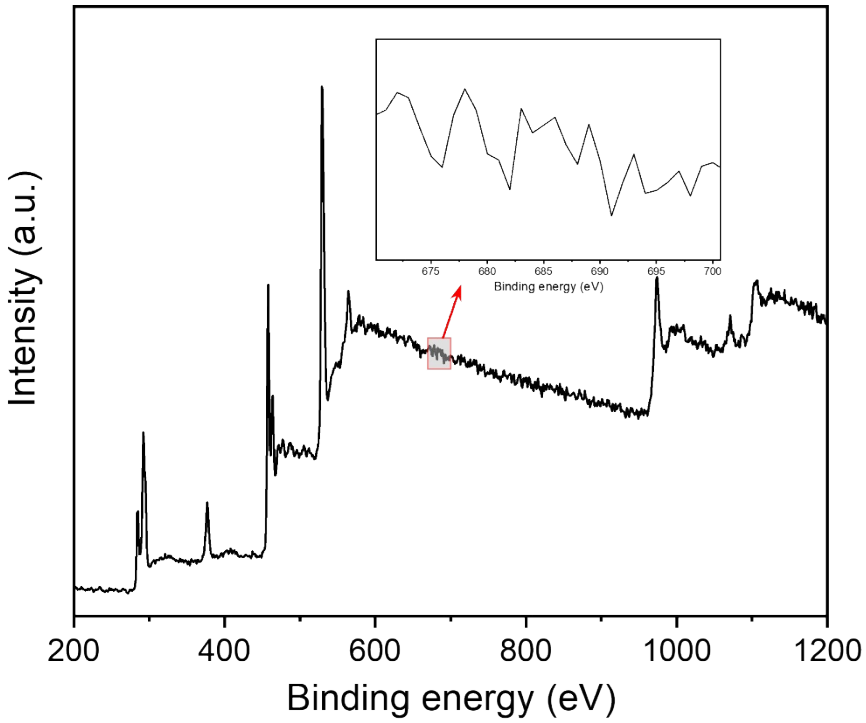

Figure S8. XPS survey spectrum of GB-TiO_2 with the enlarged region of the F 1s signal, indicating the absence of fluorine residues after synthesis.

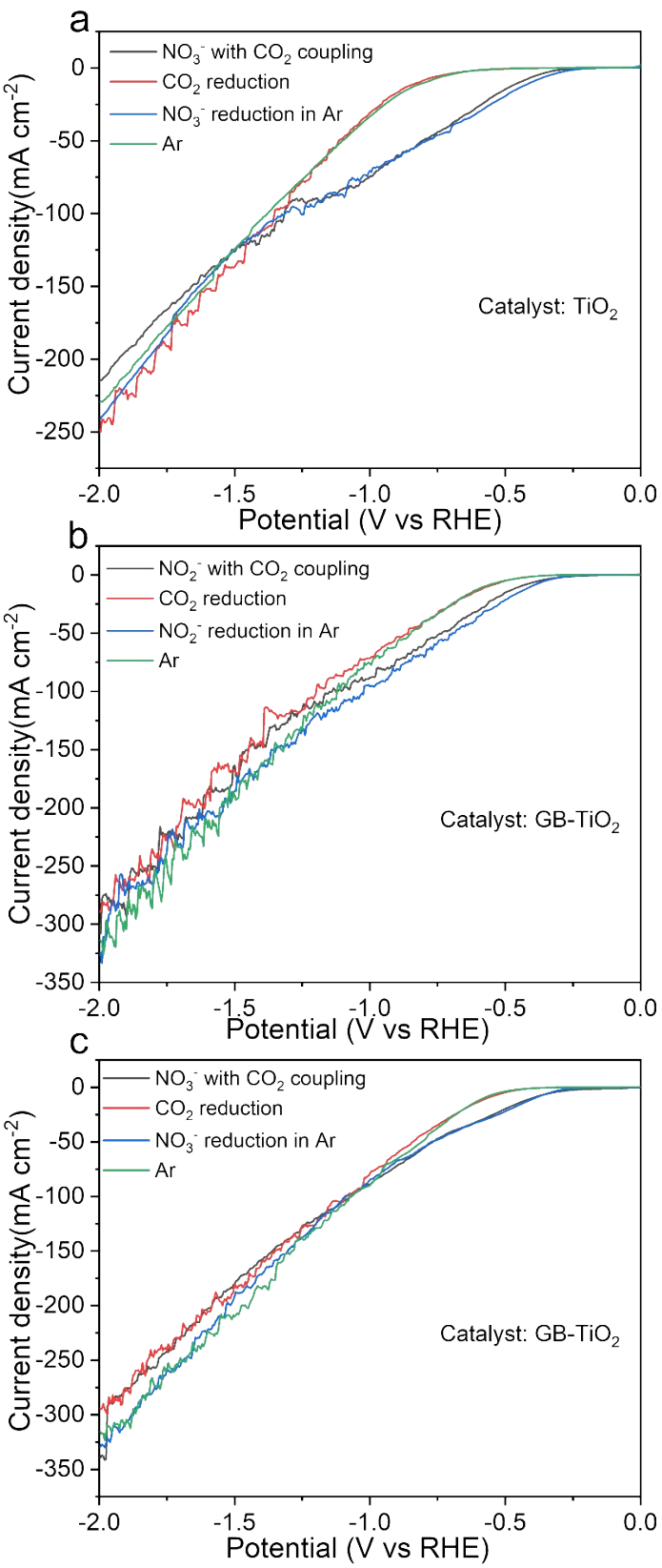

Figure S9. (a, b) LSV curves of TiO_2 and GB-TiO_2 under Ar, CO_2, NO_2^- in Ar and NO_2^- in CO_2. (c) LSV curves of GB-TiO_2 after poisoning.

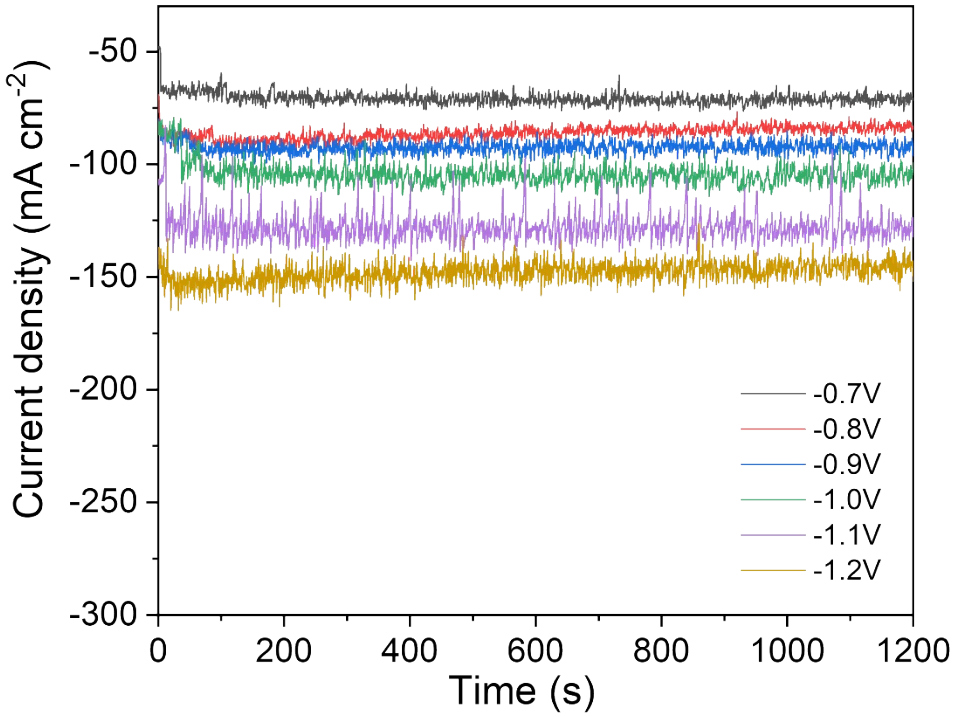

Figure S10. I-t curves for electrocatalytic urea synthesis at various applied potential on GB-TiO_2.

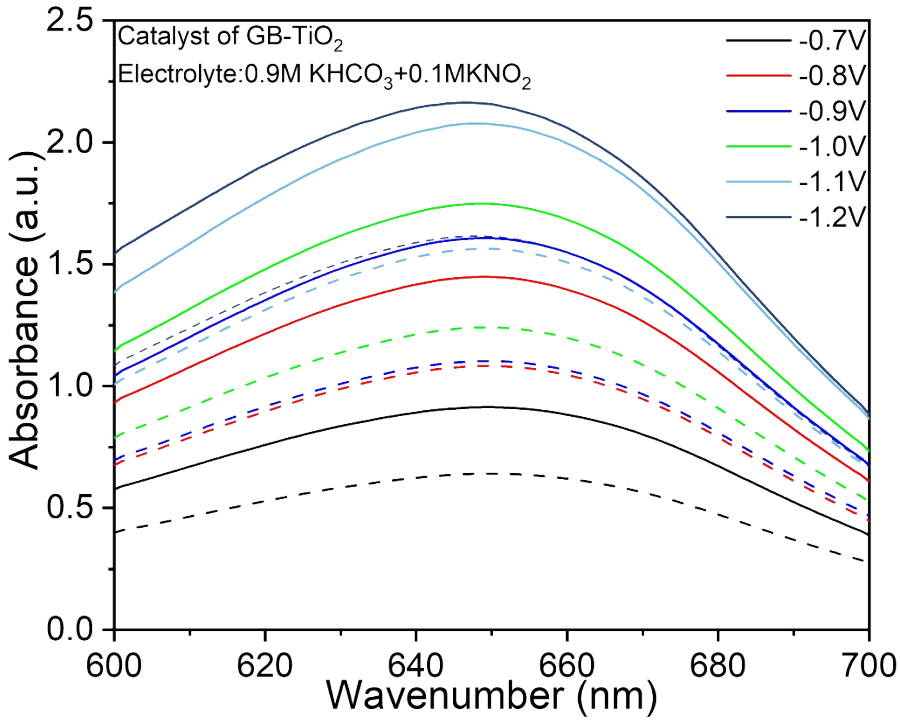

Figure S11. The UV-vis spectra before and after the addition of urease at different potentials of GB-TiO_2. (The dotted line and solid line represent before and after urease decomposition respectively.)

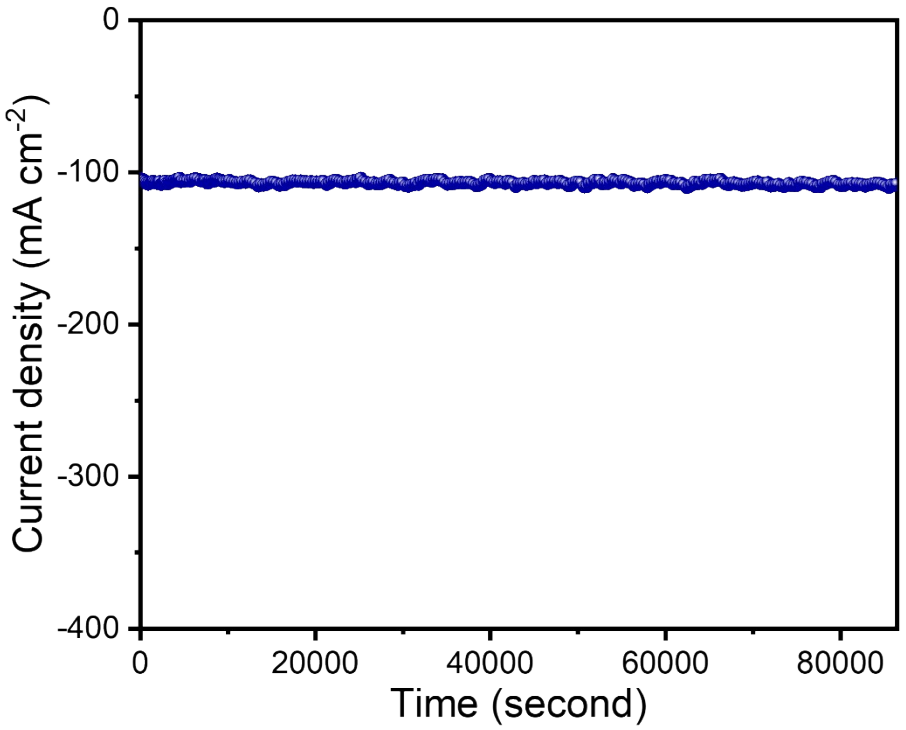

Figure S12. Chronoamperometric curves of GB-TiO_2 at – 0.9 V versus RHE for continuous co-electrocatalytic measurements

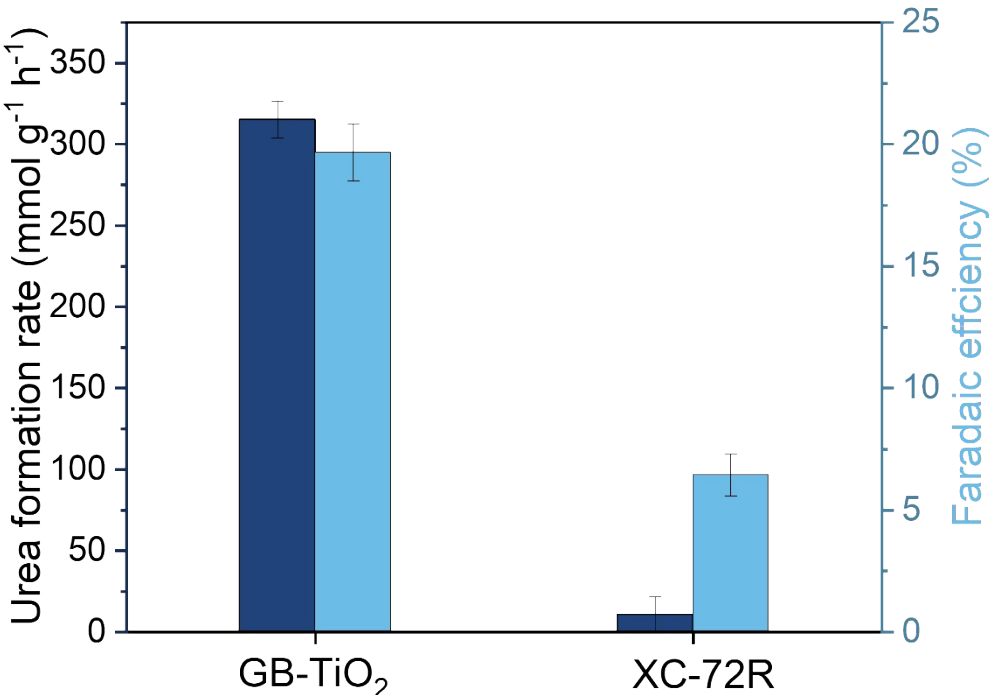

Figure S13. Comparison of urea yield rates and corresponding Faradaic efficiencies for GB-TiO_2 and its carbon additives at – 1.0V (versus RHE).

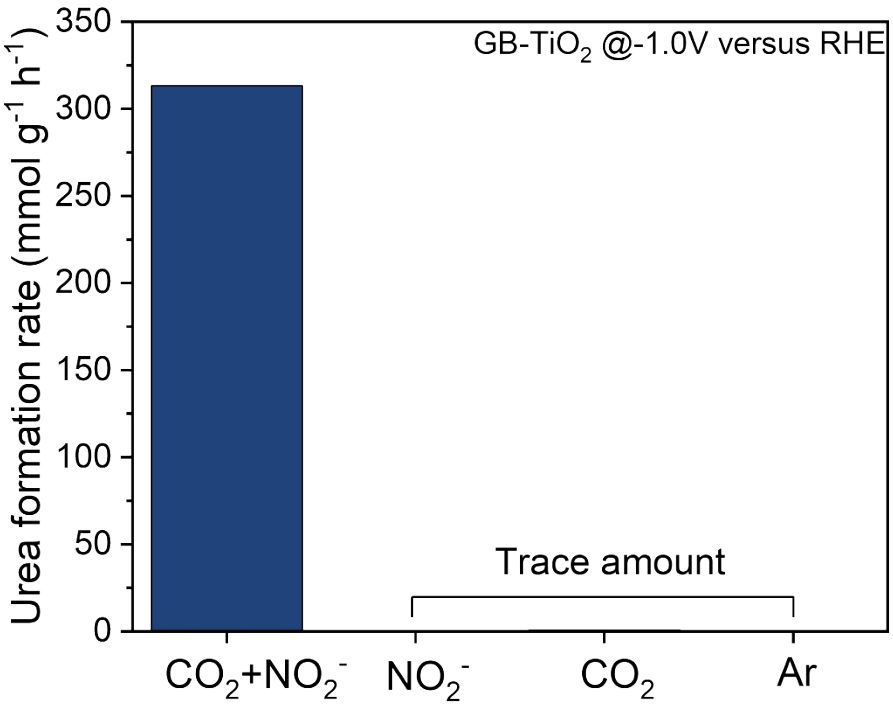

Figure S14. Contrast experiments for electrolysis of GB-TiO_2 at – 1.0 V versus RHE with different types of feedstocks.

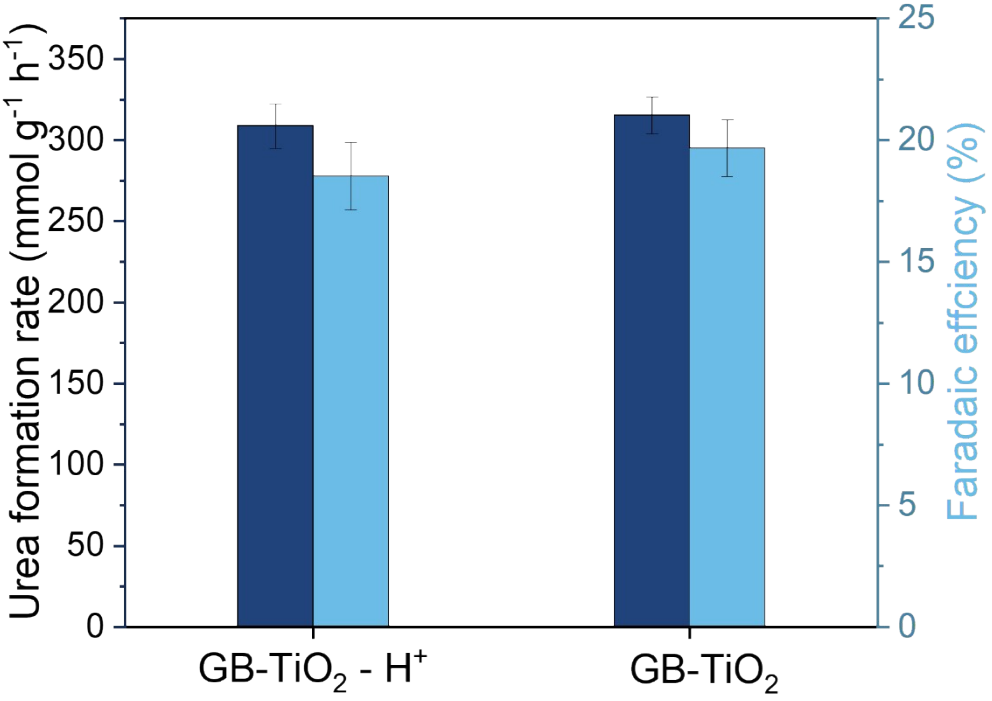

Figure S15. Comparison of urea formation rate and corresponding Faradaic efficiency over GB-TiO_2 before and after acid treatment to remove possible surface residues.

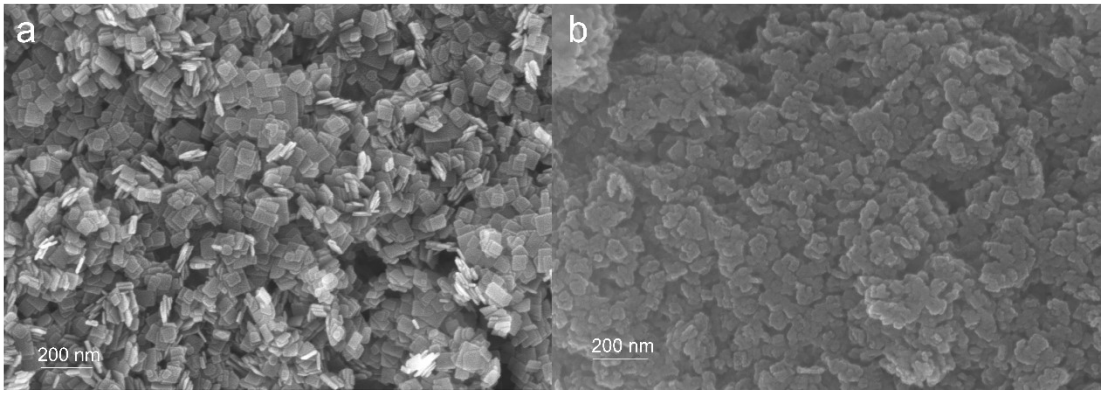

Figure S16. SEM images of TiO_2 after electrochemical stability tests.

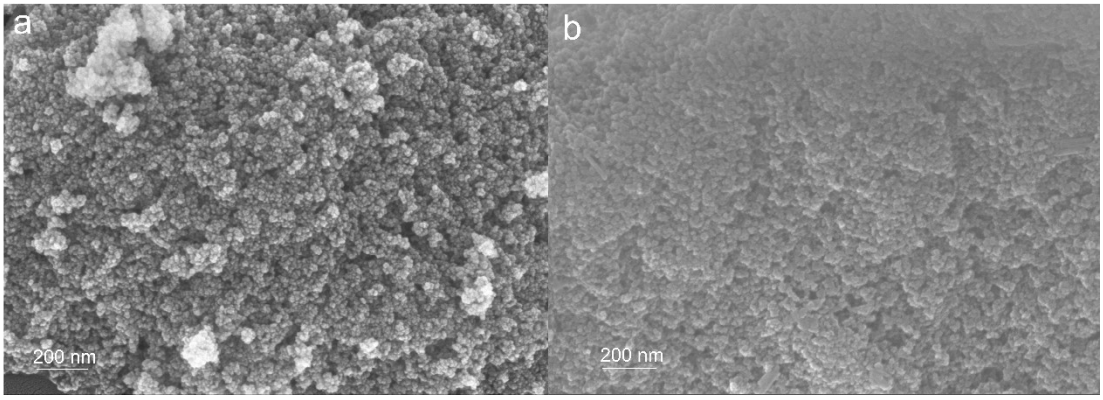

Figure S17. SEM images of GB-TiO_2 after electrochemical stability tests.

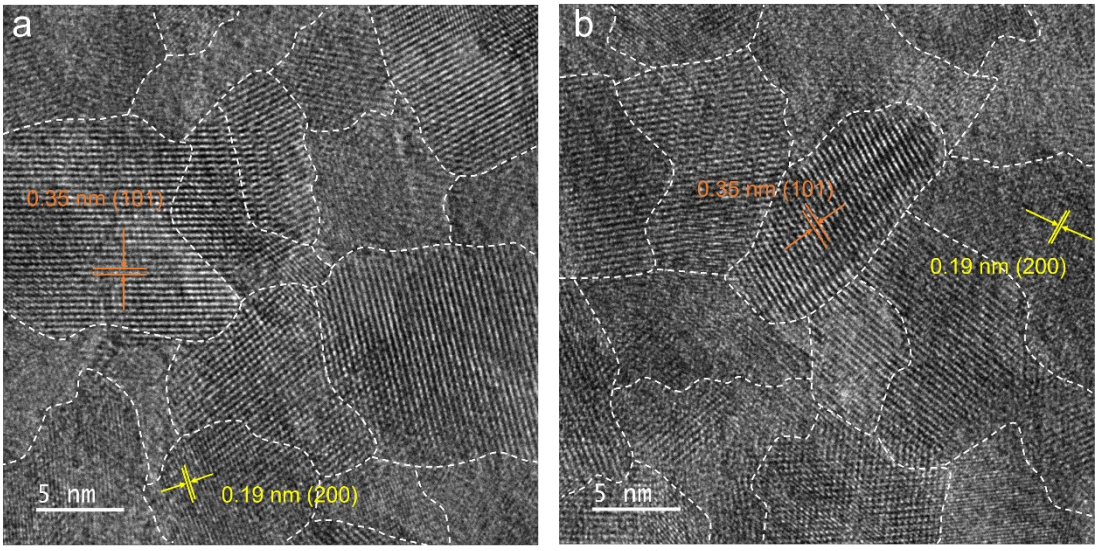

Figure S18. HRTEM images of GB-TiO_2 (a) before electrolysis and (b) after the 24 h stability test.

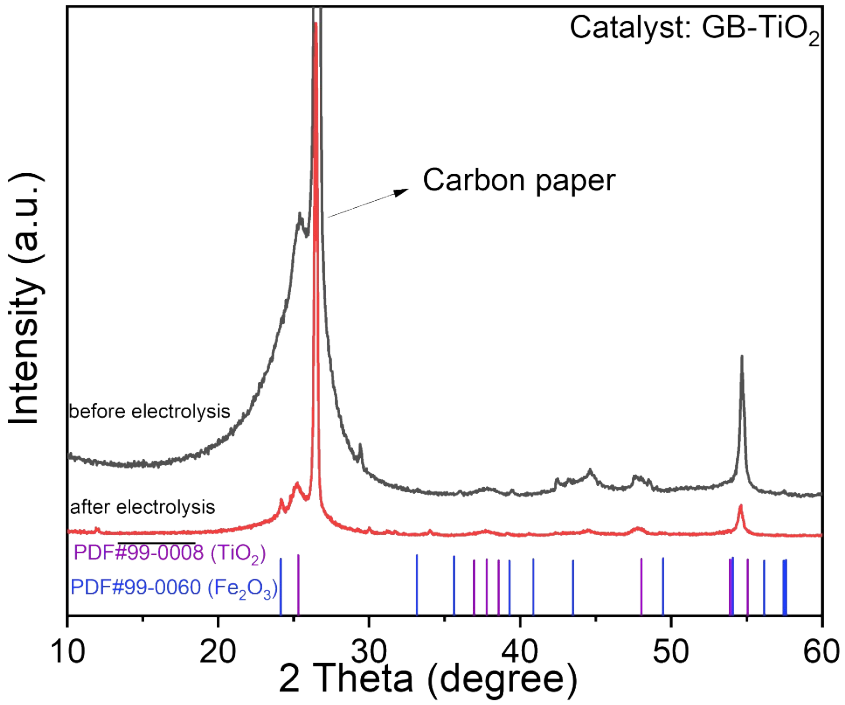

Figure S19. XRD patterns of GB-TiO_2 after electrochemical stability tests.

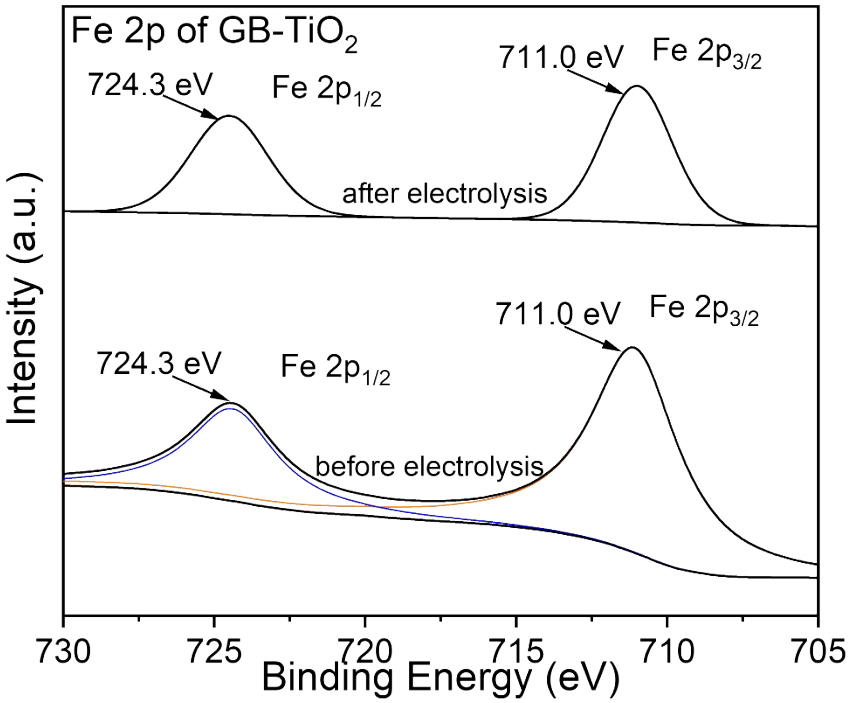

Figure S20. Fe 2p XPS spectra of GB-TiO_2 after electrochemical stability tests.

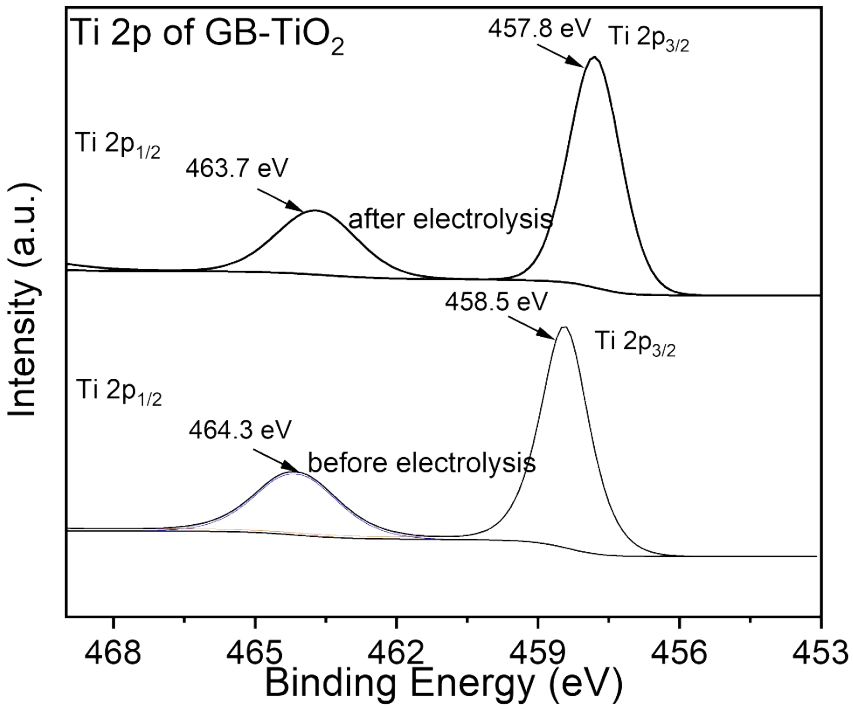

Figure S21. Ti 2p XPS spectra of GB-TiO_2 after electrochemical stability tests.

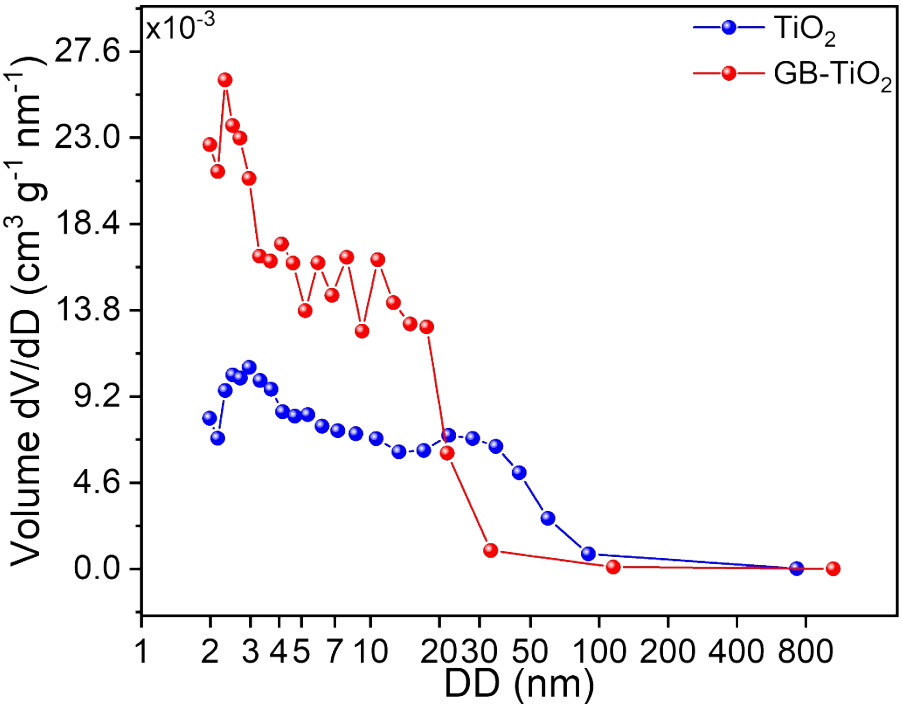

Figure S22. Adsorption-desorption curve of TiO_2 and GB-TiO_2.

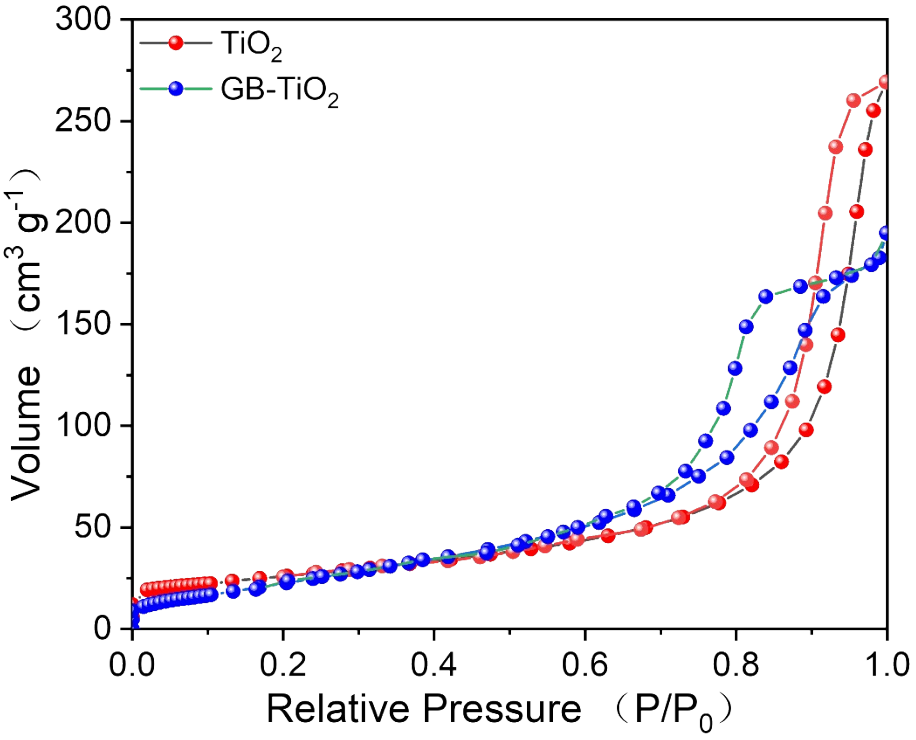

Figure S23. Nitrogen adsorption-desorption isotherms of TiO_2 and GB-TiO_2 obtained by the BET method.

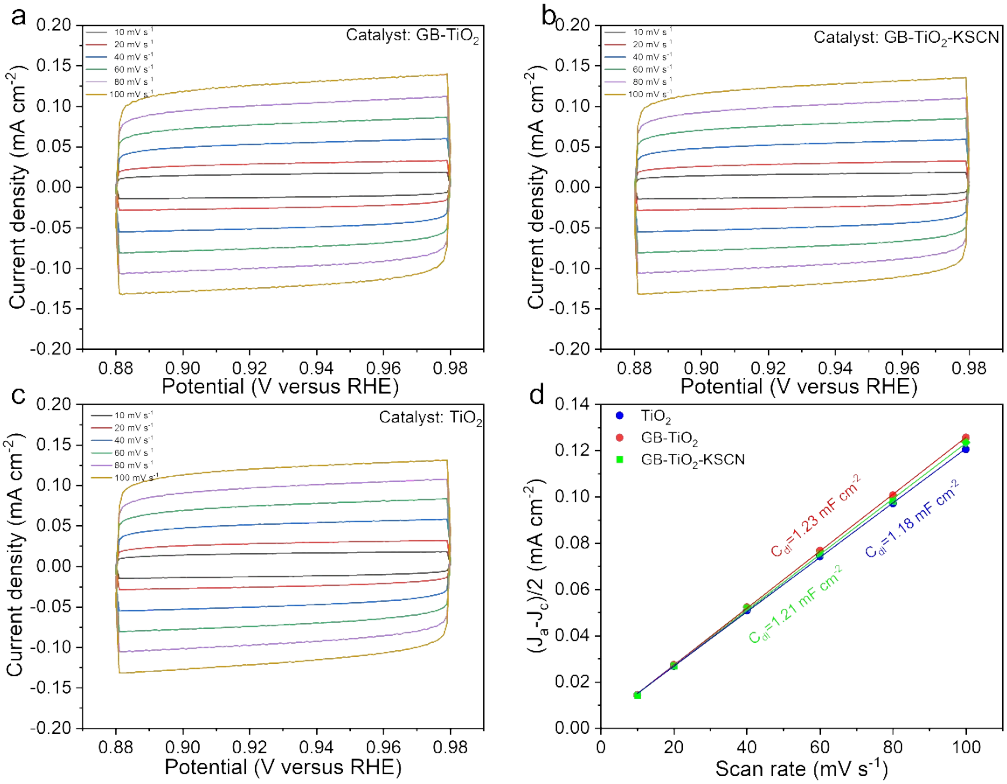

Figure S24. The measurements of double-layer capacitance of (a) GB-TiO_2, (b) GB-TiO_2-KSCN and (c) TiO_2.

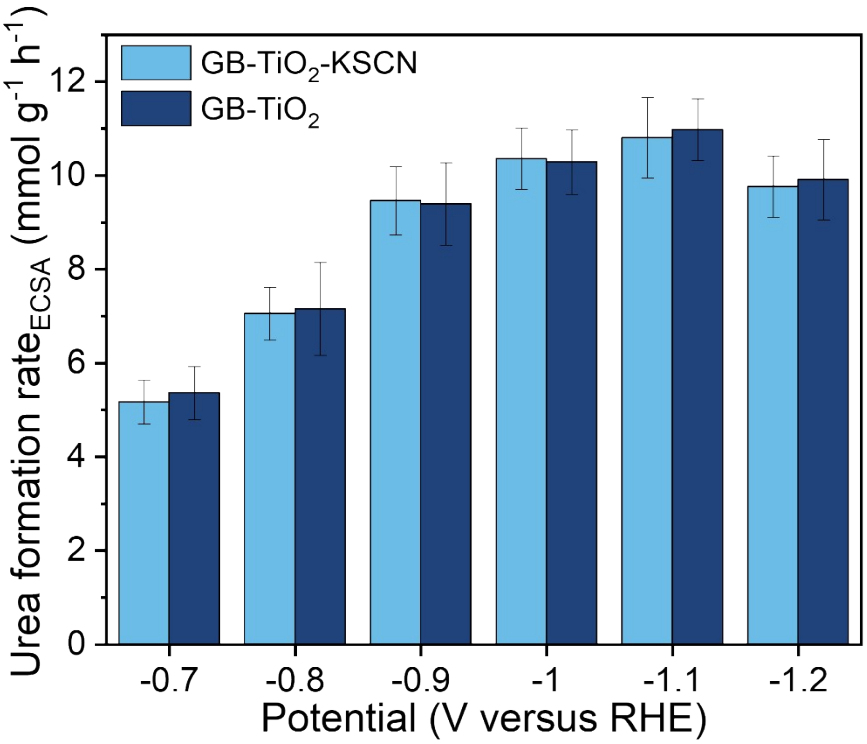

Figure S25. The urea production rate normalized by the electrochemical surface area (ECSA) before and after SCN^- poisoning.

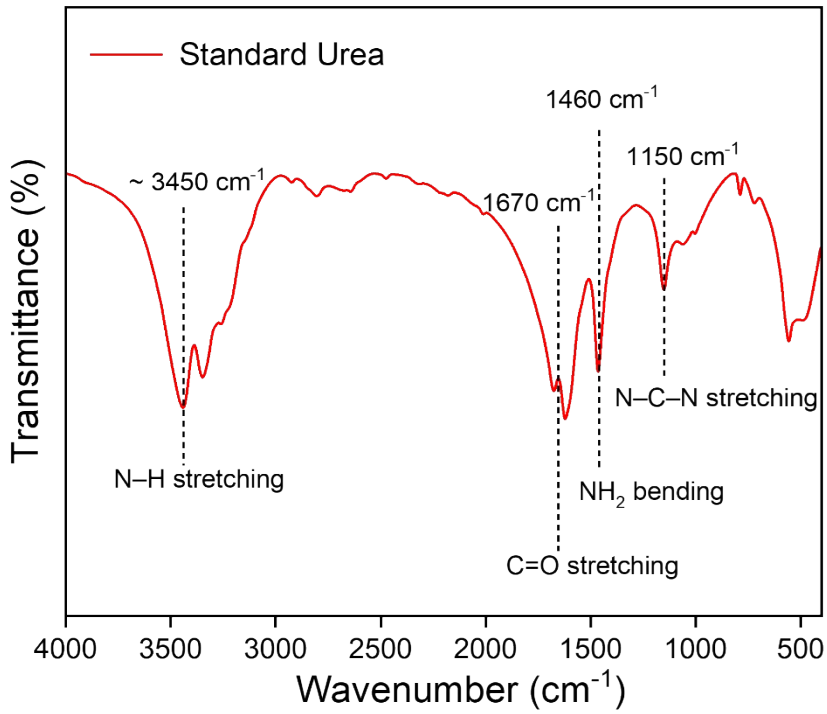

Figure S26. FTIR spectrum of standard urea, showing characteristic absorption bands in regions associated with N−H stretching (~3450 cm^{-1}), C=O stretching (1670 cm^{-1}), NH_2 bending (1460 cm^{-1}), and N−C−N stretching (1150 cm^{-1}).

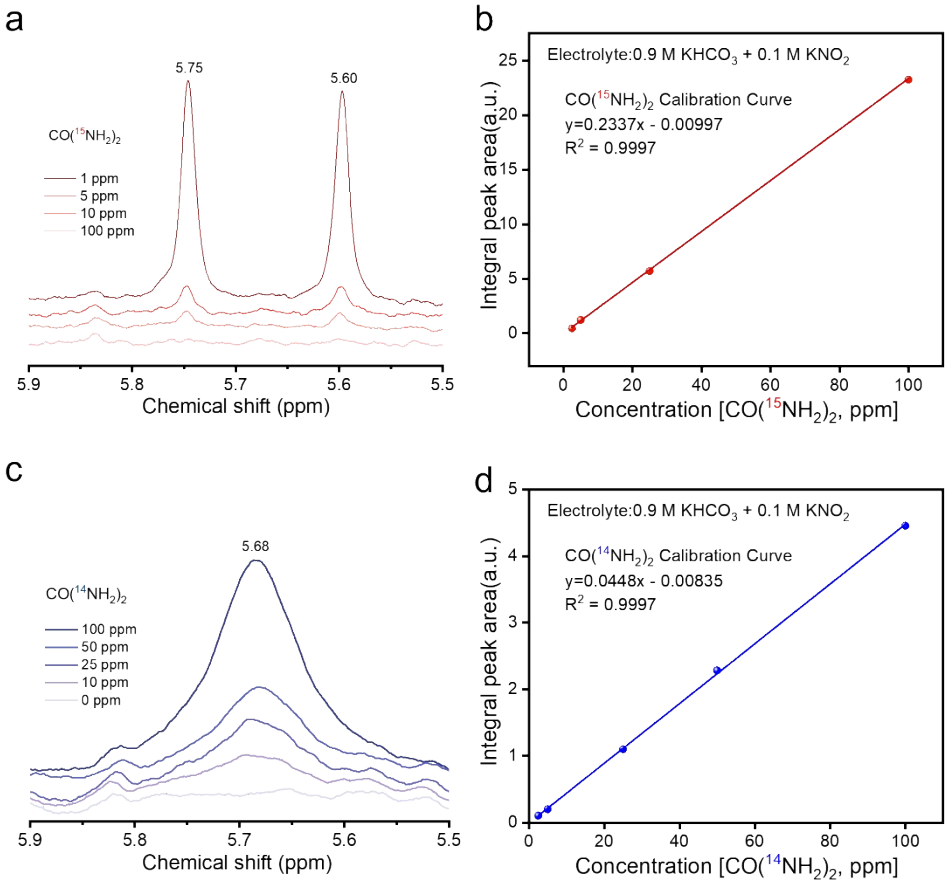

Figure S27. ^{1}H NMR spectra and corresponding calibration curves of ^{15}N-labeled urea and ^{14}N-urea in 0.9 M $KHCO_3$ + 0.1 M KNO_2 electrolyte: (a) ^{1}H NMR spectra of $CO(^{15}NH_2)_2$ at different concentrations; (b) calibration curve derived from the integrated peak area of $CO(^{15}NH_2)_2$; (c) ^{1}H NMR spectra of $CO(^{14}NH_2)_2$ at different concentrations; (d) calibration curve derived from the integrated peak area of $CO(^{14}NH_2)_2$.

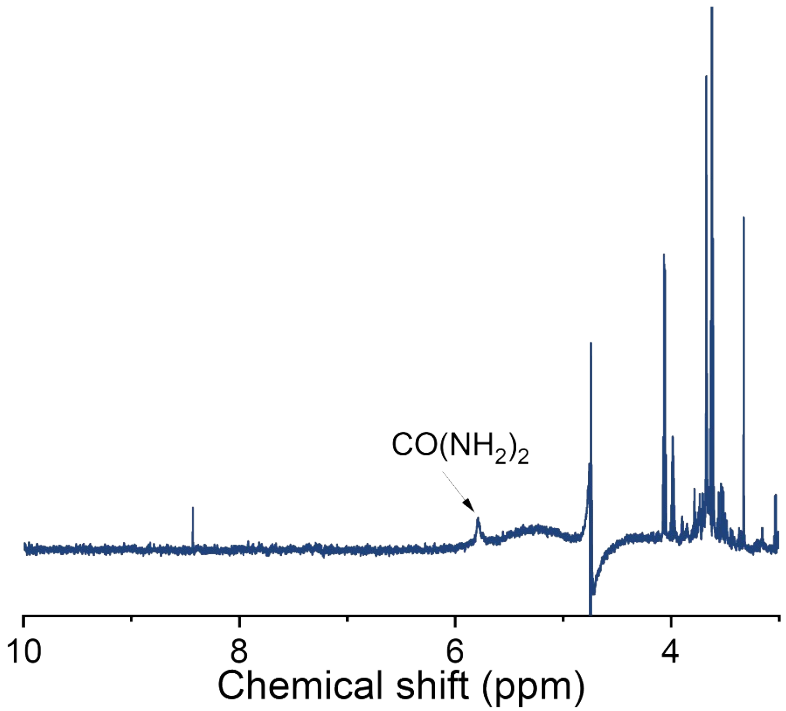

Figure S28. ^{1}H NMR spectra for electrolytes after co-electrolysis of CO_2 with NO_2^-.

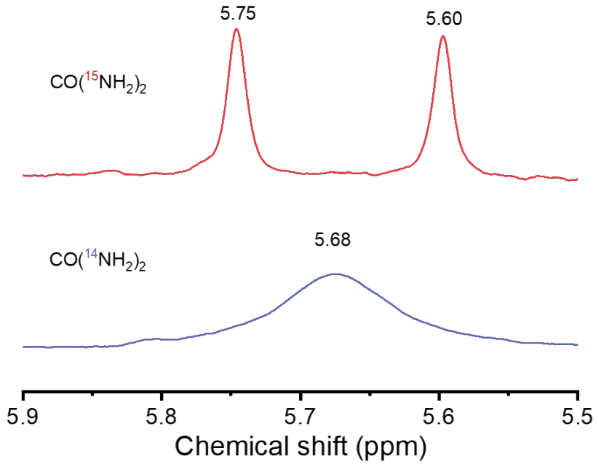

Figure S29. ^{1}H NMR spectra of urea detected in the electrolyte after electrolysis using $^{15}NO_2^-$ and $^{14}NO_2^-$ as nitrogen sources, showing the characteristic signals of $CO(^{15}NH_2)_2$ (5.75 and 5.60 ppm) and $CO(^{14}NH_2)_2$ (5.68 ppm).

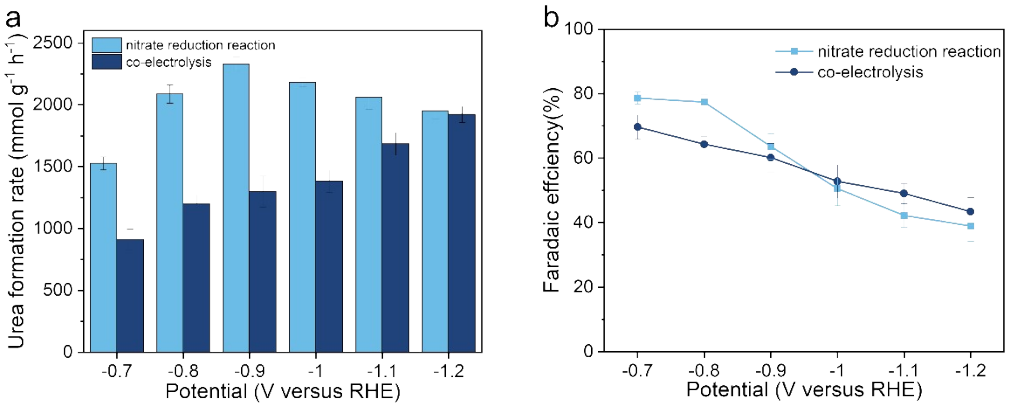

Figure S30. Ammonia yield rates and Faradaic efficiencies during nitrate reduction reaction and co-electrolysis at different applied potentials.

Table 1 Performance comparison of electrocatalytic C−N coupling for urea synthesis

N-source	Electrocatalyst	Electrolyte	Urea yield (mmol h^{-1} g^{-1})	FE(%)	Ref.
NO_2^-	GB-TiO_2	0.9 M $KHCO_3$ + 0.1 M KNO_2	317.3	19.6	This work
NO_3^-	B-FeNi-DASC	0.1 M $KHCO_3$ + 0.05 M KNO_3	20.2	17.8	[1]
	F-CNT-300	0.1 M KNO_3	6.36	18	[2]
	Vo-CeO_2-750	0.1 M $KHCO_3$ + 0.05M KNO_3	15.71	N/A	[3]
	$In(OH)_3$-S	0.1 M KNO_3	8.8	53.4	[4]
	Cu-CeO_2	0.1 M $KHCO_3$ + 0.05 M KNO_3	52.84	5.29	[5]
	$Cu_{97}In_3$-C	0.1 M $KHCO_3$ + 0.01 M KNO_3	13.1	N/A	[6]
	m-Cu_2O	0.1 M $KHCO_3$ + 0.01 M KNO_3	29.2	9.43	[7]
	Fe@C-Fe_3O_4/CNTS	0.1 M KNO_3	22.355	16.5	[8]
	Mo-PCN-222(Co)	0.1 M $KHCO_3$ + 0.05 M KNO_3	14.07	33.9	[9]
	RuCu	0.1 M KNO_3	26.81	34.82	[10]
	TiO_2	0.9 M $KHCO_3$ + 0.1 M KNO_3	265.6	26.4	[11]
	CuPc-Amino	0.1 M $KHCO_3$ + 0.05 M KNO_3	103.1	N/A	[12]
	45nm-Cu_2O	0.1 M $KHCO_3$ + 0.05 M $NaNO_3$	34.6	N/A	[13]
	CuSn/CS-1	0.1 M KNO_3	154.50	61.42	[14]
	Cu/PI-500	0.9 M $KHCO_3$ + 0.1 M KNO_3	255.0	14.3	[15]
	In-CeO_2/CP (0.05In-CeO_2)	0.1 M KNO_3	11.03	60.53	[16]
	Ag NWs@CuNi$(OH)_2$	0.1 M $KHCO_3$ + 0.1 M KNO_3	36.1	36.2	[17]

Continued Table1 Performance comparison of electrocatalytic C−N coupling for urea synthesis

N-source	Electrocatalyst	Electrolyte	Urea yield (mmol h^{-1} g^{-1})	FE(%)	Ref.
NO_2^-	Cu-TiO_2	0.2 M $KHCO_3$ + 0.02 M KNO_2	20.8	43.1	[18]
	m-Cu_2O	0.1 M $KHCO_3$ + 0.1 M KNO_2	114	11.3	[7]
	Te-doped Pd	0.1 M $KHCO_3$ + 0.01 M KNO_2	N/A	12.2	[19]
	AuCu SANF	0.5 M $KHCO_3$ + 0.01 M KNO_2	64.82	24.7	[20]
	W_1/MoS_2	0.1 M $KHCO_3$ + 0.1 M KNO_2	14.99	35.25	[21]
	Cu@Fe-N-C	0.1 M $KHCO_3$ + 100 ppm N-NO_2^-	14.16	50.05	[22]
	Cu NWs	0.02 M $NaNO_2$	15.3	96.3	[23]
	$Ru_1@Cu_3N$	0.1 M $KHCO_3$ + 0.1 M KNO_2	39.88	52.66	[24]
N_2	Pd/Cu/TiO_2-x	0.1 M $KHCO_3$	3.36	8.92	[25]
	InOOH	0.1 M $KHCO_3$	6.85	20.97	[26]
	CuPc NTs	0.1 M $KHCO_3$	2.38	12.99	[27]
	Co-PMDA-2mbIM	0.1 M $KHCO_3$	14.47	48.79	[28]
	MoP	0.1 M $KHCO_3$	0.21	36.5	[29]
	$Ni(BO_3)_2$-150	0.1 M $KHCO_3$	9.7	20.36	[30]

Note: All literature-reported urea formation rates were converted to a unified unit of mmol h^{-1} g^{-1} based on the original data in the corresponding references to ensure a fair comparison.

[1] X. Zhang, Identifying and tailoring C−N coupling site for efficient urea synthesis over diatomic Fe−Ni catalyst, Nat. Commun. 13 (2022) 5337.

[2] X. Liu, P. Kumar, Q. Chen, W. Liu, J. Liu, G. Zhang, Carbon nanotubes with fluorine-rich surface as metal-free electrocatalyst for effective synthesis of urea from nitrate and CO_2, Appl. Catal., B 316 (2022) 121618.

[3] X. Wei, X. Wen, Y. Liu, C. Chen, C. Xie, D. Wang, M. Qiu, N. He, P. Zhou, W. Chen, J. Cheng, H. Lin, J. Jia, X.-Z. Fu, S. Wang, Oxygen vacancy-mediated selective C−N coupling toward electrocatalytic urea synthesis, J. Am. Chem. Soc. 144 (2022) 11530-11535.

[4] C. Lv, L. Zhong, H. Liu, Z. Fang, C. Yan, M. Chen, Y. Kong, C. Lee, D. Liu, S. Li, J. Liu, L. Song, G. Chen, Q. Yan, G. Yu, Selective electrocatalytic synthesis of urea with nitrate and carbon dioxide, Nat. Sustain. 4 (2021) 868-876.

[5] Y. Wang, S. Xia, R. Cai, J. Zhang, C. Yu, J. Cui, Y. Zhang, J. Wu, Y. Wu, Dynamic reconstruction of two-dimensional defective Bi nanosheets for efficient electrocatalytic urea synthesis, Angew. Chem., Int. Ed. 63 (2024) e202318589.

[6] Y. Liu, X. Tu, X. Wei, D. Wang, X. Zhang, W. Chen, C. Chen, S. Wang, C-bond or O-bond surface: Which one boosts electrocatalytic urea synthesis?, Angew. Chem., Int. Ed. 62 (2023) e202300387.

[7] M. Qiu, X. Zhu, S. Bo, K. Cheng, N. He, K. Gu, D. Song, C. Chen, X. Wei, D. Wang, Y. Liu, S. Li, X. Tu, Y. Li, Q. Liu, C. Li, S. Wang, Boosting electrocatalytic urea production via promoting asymmetric C−N coupling, CCS Chem. 5 (2023) 2617-2627.

[8] J. Geng, S. Ji, M. Jin, C. Zhang, M. Xu, G. Wang, C. Liang, H. Zhang, Ambient electrosynthesis of urea with nitrate and carbon dioxide over iron-based dual-sites, Angew. Chem., Int. Ed. 62 (2023) e202210958.

[9] Y. Gao, J. Wang, M. Sun, Y. Jing, L. Chen, Z. Liang, Y. Yang, C. Zhang, J. Yao, X. Wang, Tandem catalysts enabling efficient C−N coupling toward the electrosynthesis of urea, Angew. Chem., Int. Ed. 63 (2024) e202402215.

[10] S. Fu, K. Chu, M. Guo, Y. Hu, J. Zhu, Ultrasonic-assisted hydrothermal synthesis of RhCu alloy nanospheres for electrocatalytic urea production, Chem. Commun. 59

(2023) 4344-4347.

[11] X. Tu, X. Zhu, S. Bo, X. Zhang, R. Miao, G. Wen, C. Chen, J. Li, Y. Zhou, Q. Liu, D. Chen, H. Shao, D. Yan, Y. Li, J. Jia, S. Wang, A universal approach for sustainable urea synthesis via intermediate assembly at the electrode/electrolyte interface, Angew. Chem., Int. Ed. 62 (2023) e202317087.

[12] H. Li, L. Xu, S. Bo, Q. Guo, C. Song, W. Hong, X. Li, H. Liu, W. Zhang, H. Jiang, Y. Du, J. Li, C. Chen, Ligand engineering towards electrocatalytic urea synthesis on a molecular catalyst, Nat. Commun. 15 (2024) 8858.

[13] J. Zhao, Y. Yuan, F. Zhao, X. Gao, H. Ma, Y. Huang, Q. Liu, G. Zhang, Identifying the facet-dependent active sites of Cu_2O for selective C−N coupling toward electrocatalytic urea synthesis, Energy Environ. Sci. 16 (2023) 2611-2620.

[14] X. Wu, Y. Chen, B. Tang, Q. Yan, D. Wu, H. Zhou, H. Wang, H. Zhang, D. He, H. Li, J. Zeng, L. Lu, S. Yang, T. Ma, CeO_x-integrated dual site enhanced urea electrosynthesis from nitrate and carbon dioxide, Nat. Commun. 16, 8785 (2025).

[15] Y. Wang, X. Zhu, Q. An, X. Zhang, X. Wei, C. Chen, H. Li, D. Chen, Y. Zhou, Q. Liu, H. Shao, S. Wang, Electron deficiency is more important than conductivity in C−N coupling for electrocatalytic urea synthesis, Angew. Chem. Int. Ed. 2024, 63, e202410938.

[16] Y. Zhou, S. Li, Y. Jin, R. Yang, P. Luo, C. Feng, Z. Yang, A. Abudula, P. Wang, W. Lian, G. Guan, In-situ growth of indium-doped cerium oxide for highly selective urea electrosynthesis from nitrate and carbon dioxide, Green Chem., Accepted Manuscript, 2025, DOI: 10.1039/D5GC04834F.

[17] F. Wu, F. Wu, S. Zhao, Y. Zhang, K. Zheng, L. Chen, X. Li, P. Gao, Z. Ju, W. Ye, Electrochemical tandem C−N coupling toward efficient urea synthesis enabled on highly exposed metal hydroxide interface, Cell Rep. Phys. Sci. 6 (2025) 102970.

[18] N. Cao, Y. Quan, A. Guan, C. Yang, Y. Ji, L. Zhang, G. Zheng, Oxygen vacancies enhanced cooperative electrocatalytic reduction of carbon dioxide and nitrite ions to urea, J. Colloid Interface Sci. 577 (2020) 109-114.

[19] Y. Feng, H. Yang, Y. Zhang, X. Huang, L. Li, T. Cheng, Q. Shao, Te-Doped Pd nanocrystal for electrochemical urea production by efficiently coupling carbon

dioxide reduction with nitrite reduction, Nano Lett. 20 (2020) 8282-8289.

[20] S. Liu, S. Yin, Z. Wang, Y. Xu, X. Li, L. Wang, H. Wang, AuCu nanofibers for electrosynthesis of urea from carbon dioxide and nitrite, Cell Rep. Phys. Sci. 3 (2022) 100869.

[21] D. Yuan, Y. Jiang, W. Du, D. Ma, K. Chu, Efficient urea electrosynthesis from nitrite and CO_2 reduction on single W atom catalyst, J. Colloid Interface Sci. 680 (2025) 36-42.

[22] Z. Feng, L.-H. Zhang, Y. Guo, J. Guo, F. Li, F. Yu, Angew. Chem. Int. Ed. 2025, e202500262.

[23] Y. Zhang, Y. Wang, L. Han, S. Wang, T. Cui, Y. Yan, M. Xu, H. Duan, Y. Kuang, X. Sun, Nitrite electroreduction to ammonia promoted by molecular carbon dioxide with near-unity faradaic efficiency, Angew. Chem. Int. Ed. 2022, e202213711.

[24] H. Zhao, Z. Li, J. Xiang, W. Du, K. Chu, Atomically dispersed Ru on Cu_3N for electrocatalytic reduction of CO_2 and nitrite to urea, Chem. Eng. J. 496 (2024) 154256.

[25] C. Chen, X. Zhu, X. Wen, Y. Zhou, L. Zhou, H. Li, L. Tao, Q. Li, S. Du, T. Liu, D. Yan, C. Xie, Y. Zou, Y. Wang, R. Chen, J. Huo, Y. Li, J. Cheng, H. Su, X. Zhao, W. Cheng, Q. Liu, H. Lin, J. Luo, J. Chen, M. Dong, K. Cheng, C. Li, S. Wang, Coupling N_2 and CO_2 in H_2O to synthesize urea under ambient conditions, Nat. Chem. 12 (2020) 717-724.

[26] M. Yuan, H. Zhang, Y. Xu, R. Liu, R. Wang, T. Zhao, J. Zhang, Z. Liu, H. He, C. Yang, S. Zhang, G. Zhang, Artificial frustrated Lewis pairs facilitating the electrochemical N_2 and CO_2 conversion to urea, Chem Catal. 2 (2022) 309-320.

[27] J. Mukherjee, S. Paul, A. Adalder, S. Kapse, R. Thapa, S. Mandal, B. Ghorai, S. Sarkar, U. K. Ghorai, Understanding the site-selective electrocatalytic co-reduction mechanism for green urea synthesis using copper phthalocyanine nanotubes, Adv. Funct. Mater. 32 (2022) 2200882.

[28] M. Yuan, J. Chen, H. Zhang, Q. Li, L. Zhou, C. Yang, R. Liu, Z. Liu, S. Zhang, G. Zhang, Host-guest molecular interaction promoted urea electrosynthesis over a precisely designed conductive metal-organic framework, Energy Environ. Sci. 15

(2022) 2084-2095.

[29] D. Jiao, Y. Dong, X. Cui, Q. Cai, C. R. Cabrera, J. Zhao, Z. Chen, Boosting the efficiency of urea synthesis via cooperative electroreduction of N_2 and CO_2 on MoP, J. Mater. Chem. A 11 (2023) 232-240.

[30] M. Yuan, J. Chen, Y. Xu, R. Liu, T. Zhao, J. Zhang, Z. Ren, Z. Liu, C. Streb, H. He, C. Yang, S. Zhang, G. Zhang, Highly selective electroreduction of N_2 and CO_2 to urea over artificial frustrated Lewis pairs, Energy Environ. Sci. 14 (2021) 6605-6615.